iScience

CellPress
OPEN ACCESS

Article

CD200R signaling contributes to unfavorable tumor microenvironment through regulating production of chemokines by tumor-associated myeloid cells

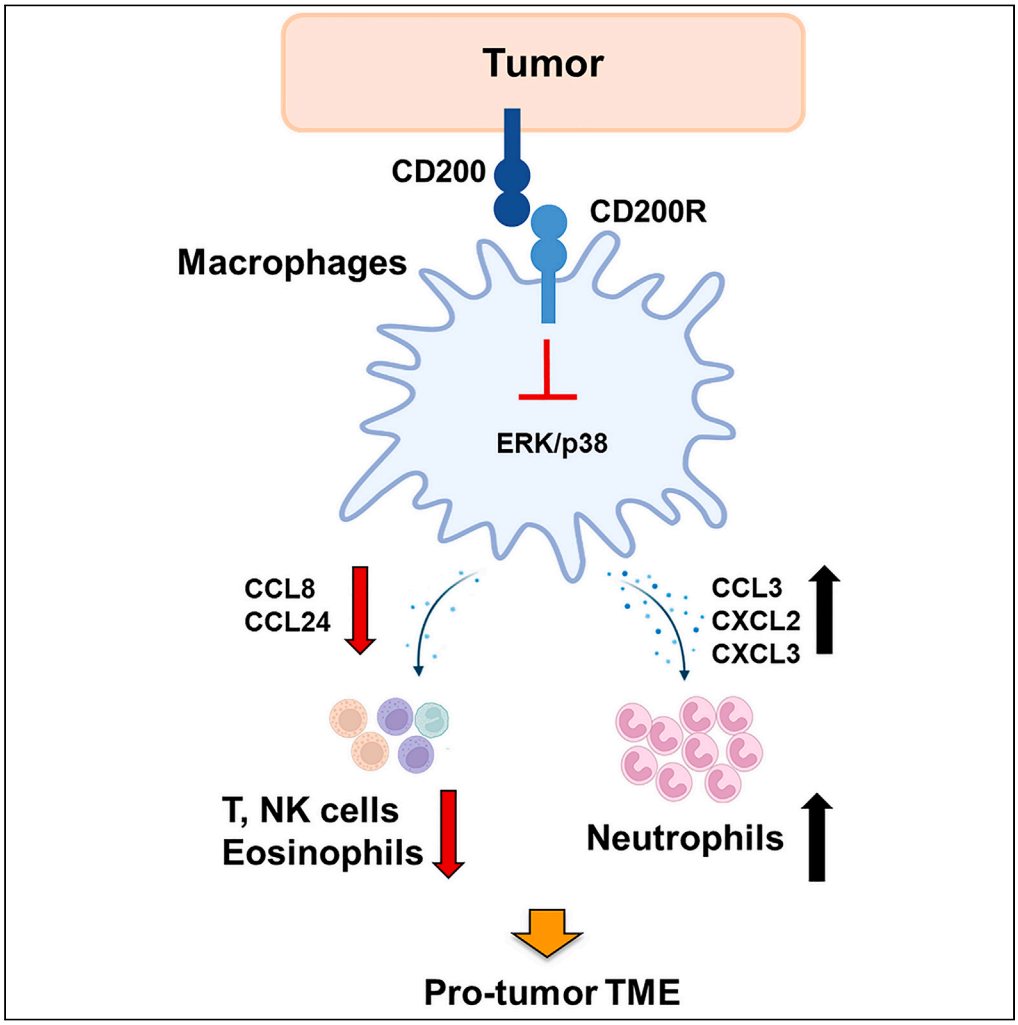

Cho-Hao Lin, Fatemeh Talebian, Yang Li, ..., Zihai Li, Qin Ma, Xue-Feng Bai

Xue-Feng.Bai@osumc.edu

Highlights

CD200 positive tumors grew significantly slower in CD200R$^{-/-}$ mice

Increased immune effectors in CD200R-deficient tumors reduces the tumor growth

CD200R signaling regulates the chemokine expression in tumor-associated myeloid cells

Eosinophils were recruited into CD200R-deficient tumors and inhibiting tumor growth

Lin et al., iScience 26, 106904
June 16, 2023
https://doi.org/10.1016/j.isci.2023.106904

iScience

CellPress
OPEN ACCESS

Article

CD200R signaling contributes to unfavorable tumor microenvironment through regulating production of chemokines by tumor-associated myeloid cells

Cho-Hao Lin,[1,8] Fatemeh Talebian,[1,8] Yang Li,[2,8] Jianmin Zhu,[1] Jin-Qing Liu,[1] Bolin Zhao,[1] Sujit Basu,[1] Xueliang Pan,[2] Xi Chen,[3] Pearlly Yan,[3] William E. Carson,[4,5] Gang Xin,[5,6] Haitao Wen,[5,6] Ruoning Wang,[5,7] Zihai Li,[5] Qin Ma,[2,5] and Xue-Feng Bai[1,5,9,*]

SUMMARY

CD200 is overexpressed in many solid tumors and considered as an immune checkpoint molecule dampening cancer immunity. In this study, we found that CD200R$^{-/-}$ mice were significantly more potent in rejecting these CD200^{+} tumors. scRNA sequencing demonstrated that tumors from CD200R$^{-/-}$ mice had more infiltration of CD4^{+} and CD8^{+} T cells, and NK cells but less infiltration of neutrophils. Antibody depletion experiments revealed that immune effector cells are crucial in inhibiting tumor growth in CD200R$^{-/-}$ mice. Mechanistically, we found that CD200R signaling regulates the expression of chemokines in tumor-associated myeloid cells (TAMCs). In the absence of CD200R, TAMCs increased expression of CCL24 and resulted in increased infiltration of eosinophils, which contributes to anti-tumor activity. Overall, we conclude that CD200R signaling contributes to unfavorable TME through chemokine-dependent recruitment of immune suppressive neutrophils and exclusion of anti-cancer immune effectors. Our study has implications in developing CD200-CD200R targeted immunotherapy of solid tumors.

INTRODUCTION

CD200 and CD200R are transmembrane glycoproteins belonging to the immunoglobulin superfamily of proteins (IgSF). CD200 has a small 19aa intracellular domain with no known signaling motif.[1] CD200R, the cognate receptor of CD200, is primarily expressed in myeloid cells.[2] Unlike most of the IgSF receptors, CD200R lacks immunoreceptor tyrosine-based inhibitory motif (ITIM) motif.[3] However, its cytoplasmic domain contains three tyrosine residues, and the third tyrosine residue is phosphorylated upon ligation of the CD200R.[4] This leads to the recruitment and phosphorylation of Dok-2 and 1, which then bind to RasGAP and SHIP.[4–6] In myeloid cells, this cascade has been shown to inhibit the phosphorylation of ERK, p38, and JNK,[5] thereby inhibiting myeloid cell activation.[7] CD200R signaling in macrophages appears to limit autoimmune inflammation in animal models of multiple sclerosis and arthritis,[8] and lung injury caused by viral infection.[9] CD200R-deficient mice were also more susceptible to arthritis, due to enhanced macrophage functions.[10] These findings suggest that the CD200-CD200R pathway is mainly involved in regulating the activation of myeloid lineages of cells.

Studies have revealed that CD200 is overexpressed in human solid tumors[11] such as neuroblastoma (NB)[12] and melanoma.[13] NB is the most common non-CNS pediatric cancer, while melanoma is the most lethal type of skin cancer. Given that human NB and melanoma constitutively express CD200, the CD200-CD200R pathway is assumed to play important roles in regulating the immune microenvironment in these tumor types. Indeed, a recent study[12] has revealed that, in the tumor microenvironment (TME) of NB, CD200 is mainly overexpressed in CD45^{-} NB tumor cells, while CD200R is mainly expressed in HLA-DR^{+}CD14^{+} myeloid cells and CD11c^{+} dendritic cells. CD200-CD200R pathway appears to downregulate innate and adaptive anti-tumor immunity in the TME of NB tumors. In human melanoma, tumor expressed CD200 has been shown to inhibit T cell effector functions, and blockade of CD200 has been proposed as a therapeutic strategy for human cancer.[13,14] Thus, further studying the roles of CD200-CD200R interaction in these tumor types should reveal novel insights into the functional roles of this pathway and help developing CD200/CD200R targeted immunotherapy.

[1]Department of Pathology, College of Medicine, The Ohio State University, Columbus, OH, USA

[2]Department of Biomedical Informatics, College of Medicine, The Ohio State University, Columbus, OH, USA

[3]Genomics Shared Resource, Comprehensive Cancer Center, The Ohio State University, Columbus, OH, USA

[4]Department of Surgery, Division of Surgical Oncology, Comprehensive Cancer Center, The Ohio State University, Columbus, OH, USA

[5]Pelotonia Institute for Immuno-Oncology, Comprehensive Cancer Center, The Ohio State University, Columbus, OH, USA

[6]Department of Infection and Immunity, College of Medicine, The Ohio State University, Columbus, OH, USA

[7]Department of Pediatrics, College of Medicine, The Ohio State University, Columbus, OH, USA

[8]These authors contributed equally

[9]Lead contact

*Correspondence: Xue-Feng.Bai@osumc.edu

https://doi.org/10.1016/j.isci.2023.106904

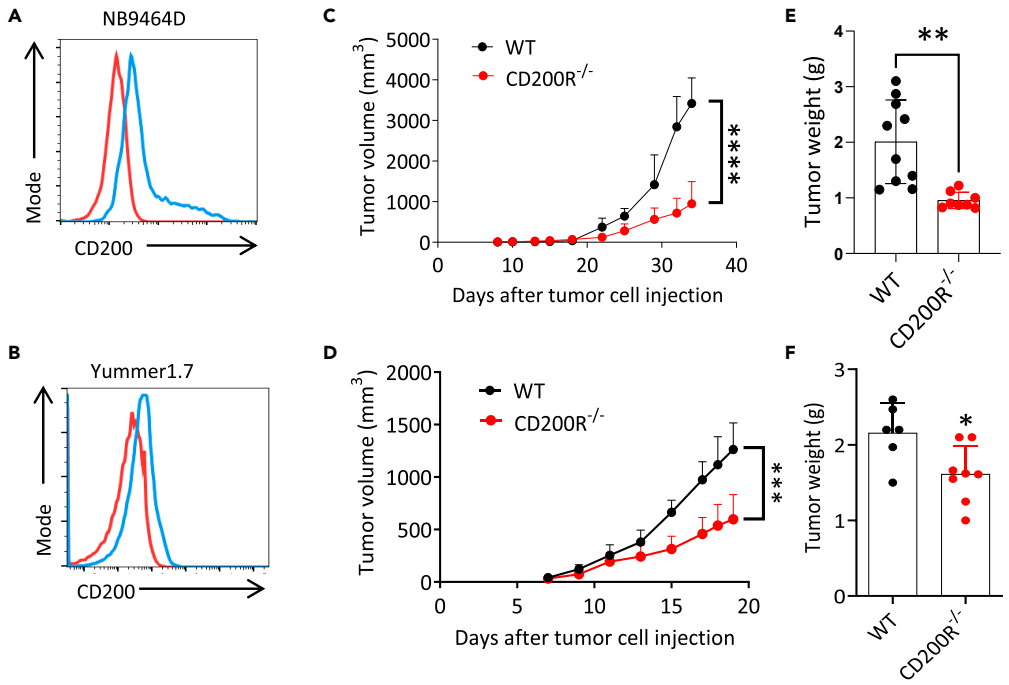

Figure 1. Reduced growth of NB9464D and Yummer1.7 tumors in CD200R$^{-/-}$ mice

(A and B) Flow cytometry analysis of CD200 expression in mouse neuroblastoma NB9464D (A) and mouse melanoma Yummer1.7 (B) cells. Red line represents isotype antibody control, blue line represents cells stained with CD200 antibody.

(C and D) Tumor growth kinetics. NB9464D (C) or Yummer1.7 (D) cells were injected into each mouse s.c. Tumor growth was monitored by measuring tumor length and width every 2 days after the appearance of tumors.

(E and F) Tumor weight plots. NB9464D (E) or Yummer1.7 (F) tumors harvested from wild type and CD200R$^{-/-}$ mice at the end of the experiments were weighted. Data shown represents three experiments with similar results. *$p < 0.05$, **$p < 0.01$, ***$p < 0.001$, ****$p < 0.0001$ by two-sided Student's *t* test.

In this study, we evaluated the role of the CD200-CD200R pathway using two murine tumor models, i.e., the mouse neuroblastoma NB9464D and the mouse melanoma Yummer1.7 models. NB9464D cells were originally derived from spontaneous NB tumors arising in tyrosine hydroxylase (TH)-MYCN transgenic mice,[15] and therefore a human-relevant mouse model. Yummer1.7 cells are the more mutated cells of Yumm1.7 that bear Braf/Pten mutations[16] resembling human melanoma. In this work, we found that in CD200R$^{-/-}$ mice, both tumor types grew significantly slower than in wild type mice. Mechanistically, we have found that CD200R signaling differentially regulates the expression of chemokines in TAMCs. In the absence of CD200R, TAMCs up-regulate CCL24 and CCL8 and down-regulate CXCL3, CXCL2, and CCL3 via activation of ERK and/or p38 MAP kinases. Increased expression of CCL24 in TAMCs resulted in increased recruitment of eosinophils, which contributes to anti-tumor activity. Thus, CD200R-mediated signaling, via interaction with CD200 on tumor cells, contributes to unfavorable TME primarily through chemokine-dependent recruitment of immune suppressive neutrophils and exclusion of anti-cancer immune effectors.

RESULTS

NB9464D and Yummer1.7 tumors grow more slowly in CD200R$^{-/-}$ mice

Human neuroblastoma and melanoma have been shown to overexpress CD200 [12,13]. We, therefore, chose neuroblastoma and melanoma mouse models to evaluate the roles of CD200R signaling in tumor growth and immunity. NB9464D cells were initially derived from mouse spontaneously developed neuroblastoma.[15] The Yumm1.7 melanoma tumor cell line was derived from a spontaneous tumor initially developed in a mouse bearing Braf/Pten mutations.[16] Additional mutations were further induced in these cells by UVB to generate Yummer1.7 cells making the model more immunogenic and suitable for evaluating checkpoint inhibitors.[17] As shown in Figures 1A and 1B, both NB9464D and Yummer1.7 cells constitutively expressed CD200 on the cell surface. C57BL/6 and CD200R$^{-/-}$C57BL/6 mice were s.c. inoculated with NB9464D or Yummer1.7 cells. About two weeks after injection of NB9464D cells, tumors started to form in WT and

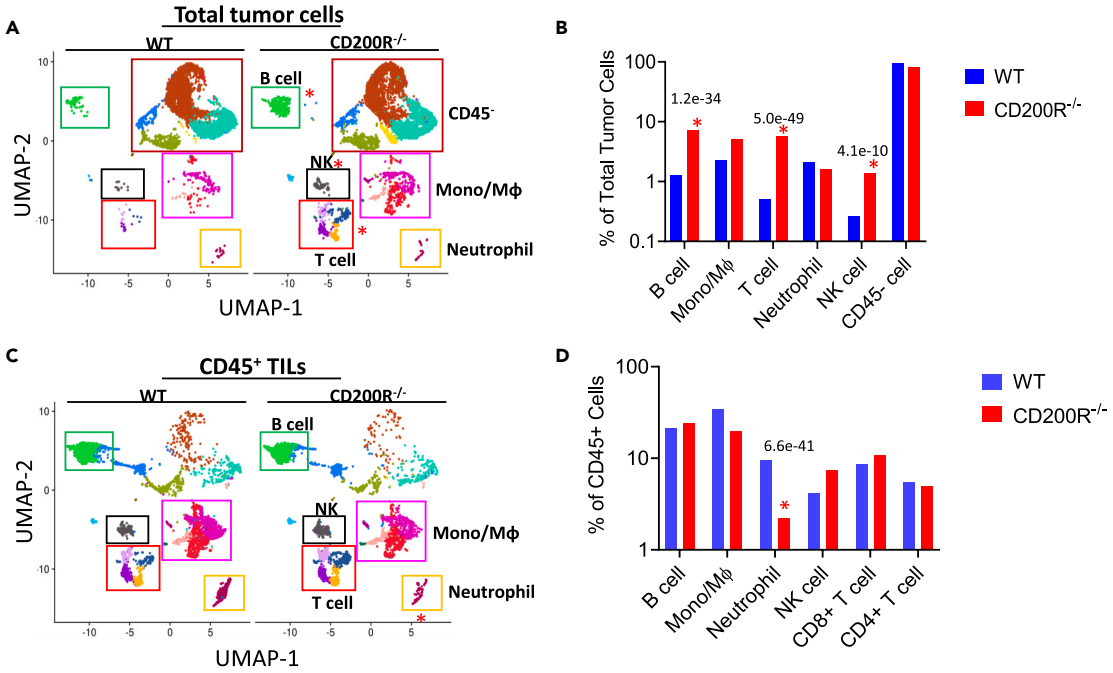

Figure 2. Single cell RNAseq analysis of tumors from WT and CD200R$^{-/-}$ mice

10 x single cell RNA-seq assays were performed on pooled total single cell samples and sorted CD45^{+} cells from NB9464D tumors grown in WT (n = 3) and CD200R$^{-/-}$ (n = 4) mice.

(A) U-MAP showing cell clusters of total cells in tumors from WT and CD200R$^{-/-}$ mice. Major populations of cells are marked by squares of different colors.

(B) Quantification of cell clusters marked by squares in A. Data were normalized to % of total cells under each condition. *P < 1e^{-10} by two proportion *z*-test.

(C) U-MAP of annotated cell clusters of sorted CD45^{+} cells from WT and CD200R-deficient tumors. Major immune cell subpopulations are marked by different colors and squares.

(D) Quantification of cell clusters marked by squares in C. Data were normalized to % of total cells under each condition. *P < 1e^{-10} by two proportion *z*-test.

CD200R$^{-/-}$ mice (Figure 1C). However, NB9464D tumors grew significantly slower in CD200R$^{-/-}$ mice than in their WT counterpart, as measured by smaller tumor volume (Figure 1C). At the end of the experiment (day 35 after tumor cell injection), we sacrificed mice and measured tumor weight and found that tumors from CD200R$^{-/-}$ mice weighed significantly less compared with tumors harvested from WT mice (Figure 1E). Similarly, we found that Yummer1.7 tumors also grew significantly slower in CD200R$^{-/-}$ mice than in WT mice, which is reflected by smaller tumor volumes (Figure 1D) and lower tumor weights (Figure 1F). Overall, our results suggest that the growth of CD200^{+} NB9464D and Yummer1.7 melanoma tumors is impaired when CD200R signaling is absent.

Increased infiltration of immune effectors but reduced infiltration of neutrophils in tumors from CD200R$^{-/-}$ mice

To understand factors affecting differential growth of tumors in WT and CD200R$^{-/-}$ mice, 10 x single cell RNAseq assays were performed on pooled total single cell samples and sorted CD45^{+} cells in NB9464D tumors from WT (n = 3) and CD200R$^{-/-}$ (n = 4) mice (GSE211963, https://www.ncbi.nlm.nih.gov/geo/query/acc.cgi?acc=GSE211963). Nineteen distinct cell populations were identified in U-MAP based on their expression of unique marker genes (Figure S1). In the U-MAP of total tumor samples, while the numbers of CD45^{-} cells were not different between WT and CD200R$^{-/-}$ tumors, total CD45^{+} cells and all its major subsets, including T, B, and NK cells, were elevated in tumors from CD200R$^{-/-}$ mice (Figures 2A and 2B). Among the CD45^{+} tumor infiltrating leukocytes, while percentages of T, B, and NK populations were not different, a significantly reduced neutrophil population was observed (Figures 2C and 2D). The findings generated by scRNA-seq analysis were verified by flow cytometry analysis. While we found significantly elevated CD45^{+} total leukocytes (Figure 3A) in tumors from CD200R$^{-/-}$ mice, the percentages of CD4^{+} and CD8^{+} T, B, and NK cells did not show a significant difference (Figure 3B) in tumors grown in WT and CD200R$^{-/-}$ mice. While the percentages of total CD11b^{+} cells among CD45^{+} leukocytes did not show a significant difference between WT and CD200R-deficient tumors (Figure 3C), the proportion

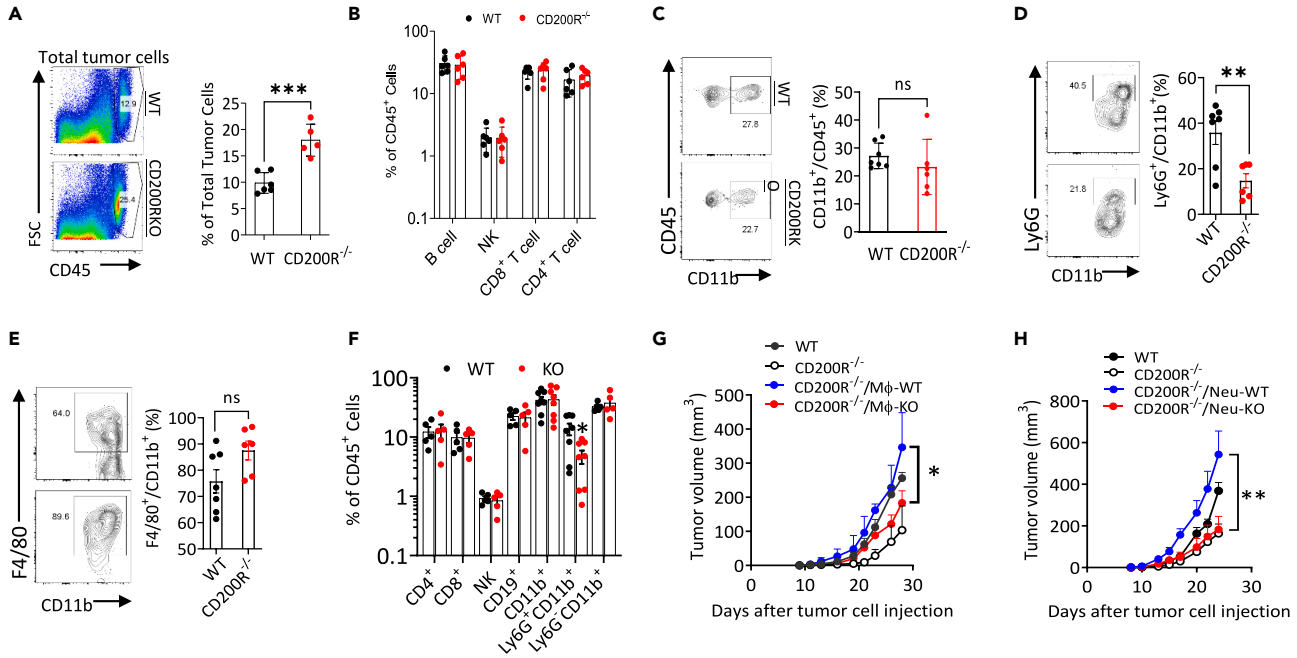

Figure 3. Flow cytometry analyses of subtypes of tumor infiltrating leukocytes and tumor promoting functions of myeloid cells

(A) Percent of CD45 positive cells in NB9464D tumors from WT and CD200R$^{-/-}$ mice were calculated relative to total tumor cells.

(B) Subsets of leukocytes in NB9464D tumors from WT and CD200R$^{-/-}$ mice were calculated relative to numbers of CD45^{+} cells.

(C) Quantification of CD11b^{+} cells among CD45^{+} population.

(D and E) Quantification of subpopulations of CD11b^{+} cells including CD11b^{+}Ly6G^{+} neutrophils (D), and F4/80^{+} cells (E) in NB9464D tumors grown in WT and CD200R$^{-/-}$ mice.

(F) Quantification of major subsets of CD45^{+} leukocytes in established Yummer1.7 tumors grown in WT and CD200R$^{-/-}$ mice. *p < 0.05, **p < 0.01, ***p < 0.001 by two-sided student's *t* test. Data shown represents three to five experiments with similar results.

(G) Bone marrow derive macrophages (BMDMs) were generated from WT or CD200R$^{-/-}$ mice and were mixed with NB9464D cells at 1:1 ratio, and 6 million mixed cells or 3 million NB9464D cells were injected into each recipient mouse s.c. n = 5–6 mice/group were used for the experiment. *p < 0.05 by one-way ANOVA.

(H) Bone marrow ly6G^{+} cells from WT or CD200R$^{-/-}$ mice were mixed with NB9464D cells at 1:1 ratio and 6 million mixed cells or 3 million NB9464D cells were injected into each recipient mouse s.c. Six mice per group were used for the experiment. Tumor growth kinetics (average tumor volume over time) are shown. **p < 0.01 by one-way ANOVA.

of the CD11b^{+}Ly6G^{+} population was significantly reduced in CD200R-deficient tumors (Figure 3D). There was also a trend of elevation of F4/80^{+} proportion among CD11b^{+} cells from CD200R-deficient tumors (Figure 3E). Similarly, in established Yummer1.7 tumors from CD200R$^{-/-}$ mice, we also detected a reduced proportion of neutrophils (Figure 3F) but observed no significant percentage differences in other leukocyte populations between WT and CD200R-deficient tumors. To evaluate the functions of CD200R-deficient macrophages in tumor growth, we generated bone marrow derived macrophages (BMDMs) from CD200R$^{-/-}$ or WT mice and mixed them with NB9464D cells at 1:1 ratio followed by injection into CD200R$^{-/-}$ mice. As shown in Figure 3G, we found that CD200R$^{-/-}$ mice receiving WT BMDMs showed accelerated tumor growth compared to CD200R$^{-/-}$ mice receiving CD200R$^{-/-}$ BMDMs. To evaluate the functions of CD200R-deficient neutrophils in tumor growth, we isolated ly6G^{+} neutrophils in bone marrows from CD200R$^{-/-}$ or WT mice and mixed them with NB9464D cells at 1:1 ratio followed by injection into CD200R$^{-/-}$ mice. As shown in Figure 3H, while CD200R$^{-/-}$ mice receiving WT ly6G^{+} cells showed accelerated tumor growth compared to CD200R$^{-/-}$ mice, no tumor enhancement was observed in mice receiving CD200R-deficient neutrophils.

CD200R signaling regulates TAMC production of chemokines in TME

To understand the mechanisms of differential recruitment of immune cell subsets in TME of CD200R-deficient tumors, we performed differential gene expression analysis of the scRNA-seq data. Among the most significantly altered expression of genes were some chemokines. As shown in Figure 4A, CD200R-deficiency

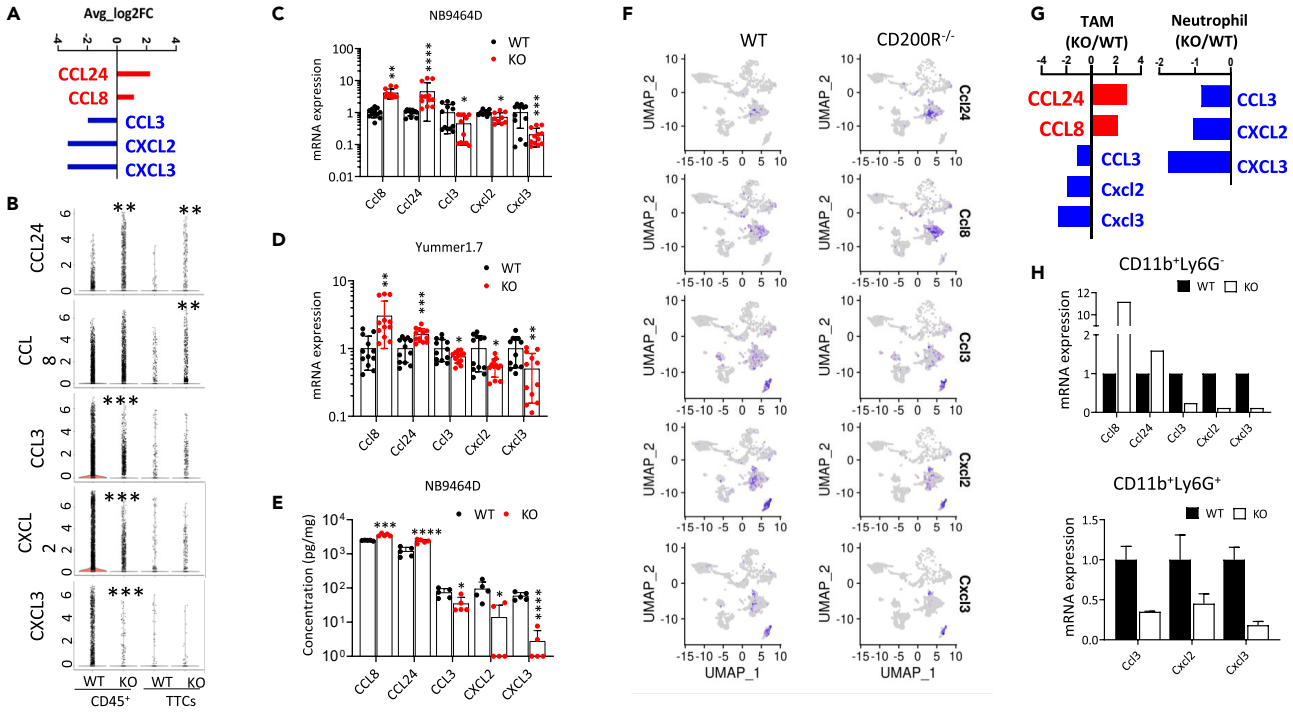

Figure 4. CD200R signaling regulates chemokine expression in TME

(A) Differential gene expression analysis of the scRNA-seq data revealed significantly altered overall expression of chemokine genes in NB9464D tumors from CD200R$^{-/-}$ mice versus tumors from WT mice.

(B) Violin plots for the expression of chemokine genes that show significant differences between tumors from WT and CD200R$^{-/-}$ mice. ***P < 1e^{-100}, **P < 1e^{-10} by Wilcoxon rank-sum test.

(C and D) qPCR analyses for the expression of chemokine genes in NB9464D (C) and Yummer1.7 (D) tumors from WT and CD200R$^{-/-}$ mice. *p < 0.05, **p < 0.01, ***p < 0.001, ****p < 0.0001 by two-sided student *t* test.

(E) ELISA assay for production of chemokines in NB9464D tumor lysates. *p < 0.05, ***p < 0.001, ****p < 0.0001 by two-sided student *t* test.

(F) Featured plot data of scRNA-seq suggests that CCL24 and CCL8 were mainly expressed by TAMs, while CCL3, CXCL2 and CXCL3 were mainly expressed by neutrophils, but also by TAMs.

(G) Differential gene expression analysis of the scRNA-seq data revealed altered expression of chemokine genes in TAMs and Neutrophils.

(H) qPCR was used to quantify expression of chemokine genes in sorted CD11b^{+}Ly6G^{-} and CD11b^{+}Ly6G^{+} cells from NB9464D tumors from WT and CD200R$^{-/-}$ mice.

resulted in a significant alteration in global expression of 5 chemokine genes, namely CCL24, CCL8, CCL3, CXCL2, and CXCL3. CCL24 and CCL8 were significantly up-regulated, while CCL3, CXCL2, and CXCL3 were down-regulated. Violin plots of the five chemokine genes suggest that these chemokines were mainly enriched in CD45^{+} leukocytes (Figure 4B). qPCR analysis confirmed the scRNA-seq data that CD200R-deficiency resulted in up-regulation of CCL24 and CCL8, downregulation of CCL3, CXCL2, and CXCL3 in both NB9464D (Figure 4C) and Yummer1.7 (Figure 4D) tumor models. Moreover, the ELISA assay also confirmed that the alteration pattern was true at the protein level (Figure 4E).

Featured plot data (Figure 4F) and differential gene expression analysis in cell subtypes (Figure 4G) revealed that CCL24 and CCL8 were mainly expressed by TAMs, while CCL3, CXCL2, and CXCL3 were mainly expressed by neutrophils, but also by TAMs. These data showed a similar pattern to the global gene expression changes. Moreover, qPCR analysis of FACS-sorted myeloid cells revealed that CD11b^{+}Ly6G^{-} cells up-regulated CCL24 and CCL8 and down-regulated CCL3, CXCL2, and CXCL3 (Figure 4H), while CD11b^{+}Ly6G^{+} cells down-regulated CCL3, CXCL2, and CXCL3 (Figure 4H).

Activation of ERK and/or p38 MAPKs mediates differential expression of chemokines in CD200R-deficient TAMCs

To determine if tumor CD200 interacts with CD200R on macrophages to regulate the production of these chemokines, we generated bone marrow derived macrophages (BMDM) from CD200R$^{-/-}$ and WT mice,

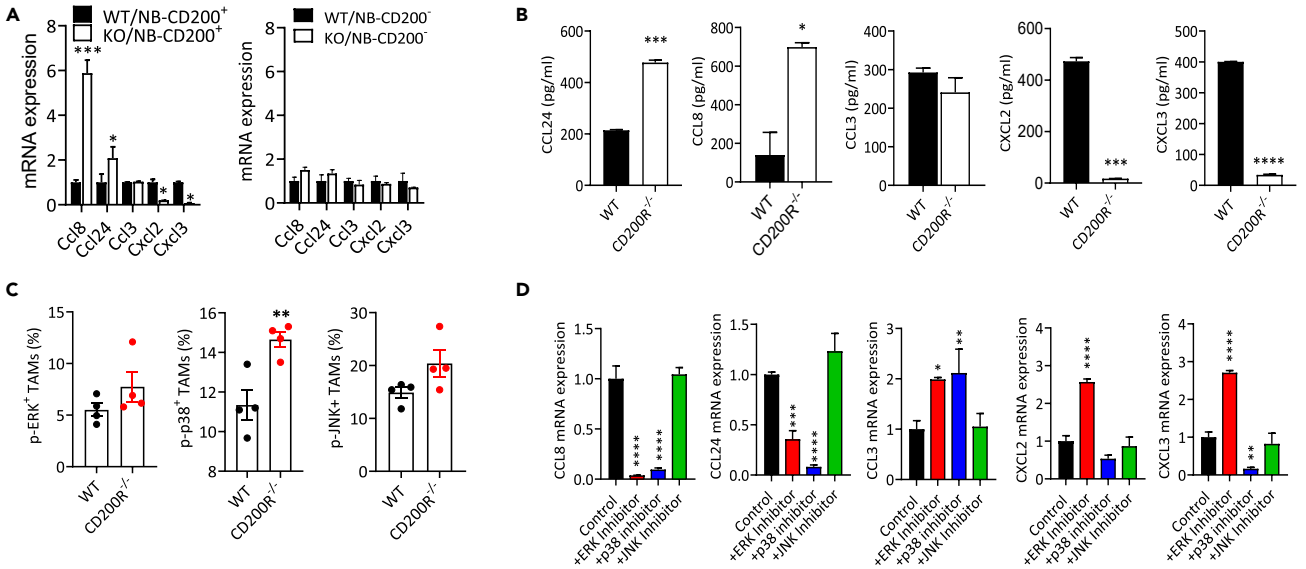

Figure 5. CD200R signaling regulates chemokine expression in BMDM through activation of ERK and/or p38 MAPKs

Bone marrow derive macrophages (BMDM) were generated and co-cultured with CD200^{+} or CD200^{-} NB9464D tumor cells.

(A) qPCR was used to quantify expression of chemokine genes in co-cultured cells. Expression of these chemokines in cultured BMDM alone was low or undetectable. Expression of these chemokine genes in NB9464D cells was undetectable.

(B) ELISA was used to quantify concentrations of chemokines produced in supernatants of co-cultures after 24 h.

(C) Levels of phospho-ERK, -p38, and -JNK in tumor-associated macrophages from NB9464D tumors were quantified by flow cytometry.

(D) inhibitors of ERK (SCH772984, 1 μM), p38 (LY2228820, 5 μM) or JNK (SP600125, 5 μM) were added to NB9464D/BMDM co-cultures. qPCR was used to quantify expression of chemokine genes in co-cultured cells. *p < 0.05, **p < 0.01, ***p < 0.001, ****p < 0.0001 by student's *t* test (A-C) or one-way ANOVA (D).

co-cultured them with CD200^{+} or CD200^{-} NB9464D tumor cells and measured expression of these chemokines. As shown in Figure 5A, CD200R-deficient BMDMs significantly up-regulated expression of CCL8 and CCL24 and downregulated expression of CXCL2 and CXCL3 genes in BMDM/CD200, but not in BMDM/CD200^{-} NB9464D co-cultures. Moreover, we found that the protein concentrations of CCL24 and CCL8 in the culture supernatants were significantly higher, while the protein concentrations of CXCL2 and CXCL3 were significantly lower in NB9464D-CD200R$^{-/-}$ macrophage co-cultures compared to NB9464D-CD200R$^{+/+}$ macrophage co-cultures (Figure 5B). In TAMCs from CD200R-deficient tumors, we detected elevated phospho-p38 and elevated trends of phospho-ERK and Phospho-JNK (Figure 5C). We, therefore, tested if inhibitors to these MAPKs would affect the expression of these chemokines. As shown in Figure 5D, we found that while inhibitors to ERK and p38 abrogated the induction of CCL24 and CCL8 in CD200R-deficient BMDMs, ERK inhibitor significantly restored the expression of CCL3, CXCL2, and CXCL3 genes in CD200R-deficient BMDMs. By contrast, inhibition of STAT or NF-kB activation did not significantly affect expression of CCL24, CCL8, CCL3, CXCL2 in the co-culture, while CXCL3 expression was slightly inhibited by NF-kB inhibitor (Figure S2). These results suggest that tumor induced activation of ERK and p38 in CD200R-deficient BMDMs enhances CCL24 and CCL8 production, while activation of ERK inhibits CCL3, CXCL2, and CXCL3 production.

Increased CCL24 expression in CD200R-deficient TAMCs recruits eosinophils into tumors, which inhibits tumor growth

CCL24 is also known as eotaxin-2, a chemokine that is mainly chemotactic to eosinophils.[18] Since CD200R-deficiency significantly enhanced CCL24 in TAMs, we analyzed if more eosinophils were recruited into CD200R-deficient tumors. As shown in Figure 6A, while we barely detected CD11b^{+}SiglecF^{+} eosinophils in NB9464D tumors from WT mice, a significant population of eosinophils was detected in tumors from CD200R-deficient mice. The eosinophil population was among the CD11b^{+} population, which comprised about 20% of CD11b^{+} cells (Figure 6B). While the spleen eosinophils from CD200R-deficient mice were of the typical SSC^{high}F4/80^{+} CCR3^{+}CCR2^{-} phenotype, tumor eosinophils downregulated CCR3 but upregulated CCR2 (Figure 6C). Similarly, we also detected elevated numbers of eosinophils in Yummer1.7 tumors

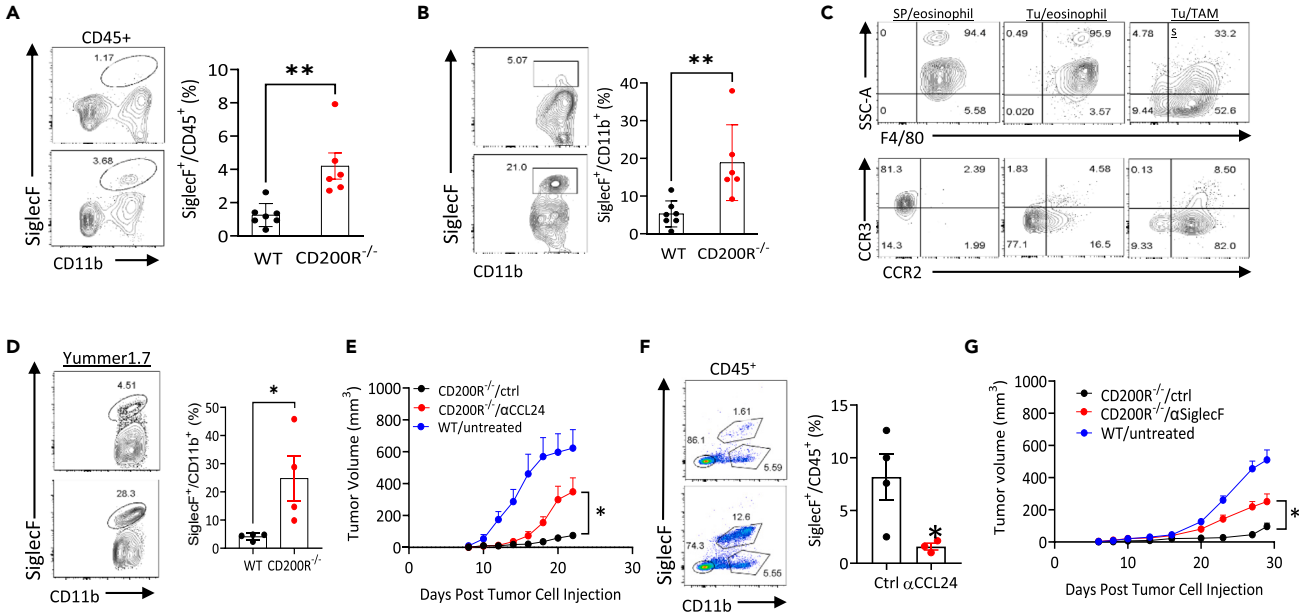

Figure 6. TAM-derived CCL24 recruits eosinophils into tumors, which inhibits tumor growth

(A and B) Percentages of eosinophils in total CD45$^+$ cells (A) and CD11b$^+$ cells (B) in NB9464D tumors grown in WT and CD200R$^{-/-}$ mice were quantified by flow cytometry. **p < 0.01 by two-sided student's *t* test.

(C) Phenotypes of eosinophils in tumors and spleens from CD200R$^{-/-}$ mice.

(D) Percentages of eosinophils among the CD11b$^+$ population in Yummer1.7 tumors grown in WT and CD200R$^{-/-}$ mice were quantified by flow cytometry. *p < 0.05 by two-sided student's *t* test.

(E) Tumor growth in CD200R$^{-/-}$ mice treated with anti-CCL24 antibody. NB9464D tumors were established in CD200R$^{-/-}$ mice followed by treatment with anti-CCL24 (n = 5) or a control Ab (n = 5). NB9464D tumors were also established in a group of WT mice for comparison.

(F) Eosinophils in tumors from anti-CCL24 treated mice and controls were quantified by flow cytometry at the end of the experiment.

(G) Tumor growth in CD200R$^{-/-}$ mice treated with anti-SiglecF antibody. NB9464D tumors were established in CD200R$^{-/-}$ mice followed by treatment with anti-SiglecF (n = 6) or a control Ab (n = 6). NB9464D tumors were also established in a group of WT mice for comparison. *p < 0.05 by two-sided student's *t* test.

grown in CD200R$^{-/-}$ mice (Figure 6D). To test if neutralizing CCL24 could affect tumor growth in CD200R$^{-/-}$ mice, we first established NB9464D tumors in CD200R$^{-/-}$ mice, followed by treatment with a CCL24 neutralizing antibody (R&D Systems, Cat#AF528). We found that anti-CCL24 treatment significantly enhanced tumor growth (Figure 6E) and caused a significant reduction of eosinophils in tumors (Figure 6F). An anti-SiglecF antibody has been shown to deplete eosinophils.[19] We, therefore, established NB9464D tumors in CD200R$^{-/-}$ mice and treated mice with anti-SiglecF. As shown in Figure 6G, anti-SiglecF antibody treatment also significantly enhanced tumor growth. These data clearly suggest that increased CCL24 expression in CD200R-deficient TAMs recruits eosinophils into tumors, which inhibits tumor growth.

Immune effector cell functions in CD200R-deficient tumors

To determine if the lack of the CD200-CD200R interaction impacted the functions of immune cells such as T and NK cells, we first examined single cell RNAseq data on the expression of major activation and effector molecules, including IFN-γ, TNF-α, PRF1, CCL5, CXCR3, GZMA, GZMB, GZMK that are typically expressed in activated T and NK cells. As shown in Figure S3, we did not find significant differences in the expression of these molecules in CD200R-deficient versus WT NK and T cells. We also evaluated the activation status and expression of effector molecules, including IFN-γ, TNF-α, Granzyme B, and perforin in infiltrating CD4$^+$ and CD8$^+$ T cells and NK1.1$^+$TCR$^-$ NK cells in NB9464D (Figures 7A–7D) and Yummer1.7 (Figures 7E–7H) tumors using flow cytometry. We also found no significant differences in the expression of these activation markers and effector molecules by T and NK cells in WT and CD200R-deficient tumors. In CD200R$^{-/-}$ mice, depletion of CD4$^+$ T cells (Figure 7I), and NK and CD8$^+$ T cells together (Figure 7J), but not CD8$^+$ T (Figure 7K) and NK (Figure 7L) cells alone, enhanced tumor growth. Thus, T and NK cells are the major immune effectors in CD200R-deficient tumors. These results suggest that CD200R-deficiency enhanced accumulation of T and NK cells in tumors but did not significantly affect their effector functions in tumors.

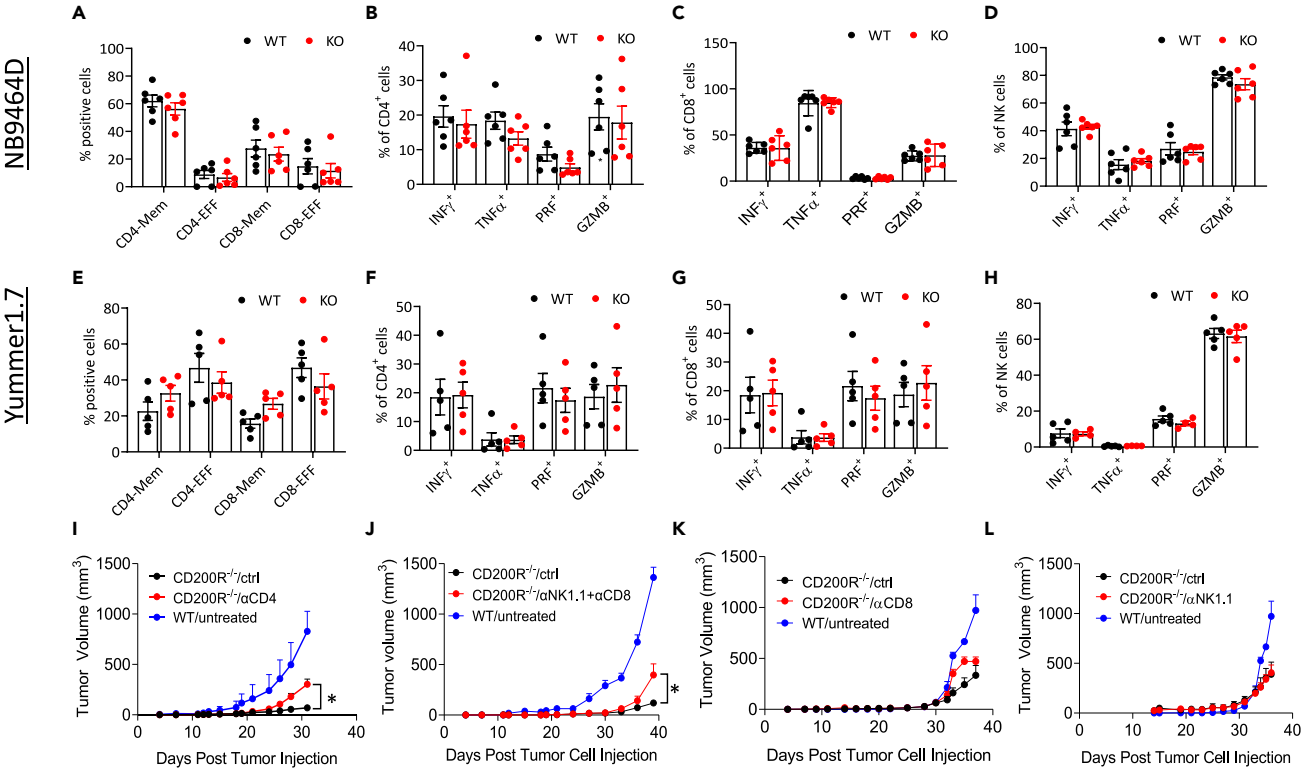

Figure 7. Immune effector cells in tumors from CD200R-deficient mice and their functional roles

Flow cytometry was used to analyze expression of immune effector molecules in tumor infiltrating $CD4^+$, $CD8^+$, or $NK1.1^+TCR^-$ NK cells.

(A–D) Percent of immune effector cells in NB9464D tumors.

(E–H) Percent of immune effector cells in Yummer1.7 tumors.

(I–L) $CD200R^{-/-}$ mice and WT were first injected with NB9464D cells to establish tumors. $CD200R^{-/-}$ mice with established tumors were then treated with anti-CD4 (I), anti-NK1.1/anti-CD8 (J), anti-CD8 (K), or anti-NK1.1 (L) antibodies or relative control antibodies. Tumor growth was monitored by measuring tumor length and width every 2 days. Tumor growth kinetics (average tumor volume over time) are shown. *$p < 0.05$ by two-sided student *t* test.

DISCUSSION

In this study, we have made a notable observation that, in the absence of CD200R signaling, TAMCs up-regulate CCL24 and CCL8 and downregulate CXCL3, CXCL2, and CCL3 via activation of ERK and/or p38 MAP kinases. Reduction of CXCL3, CXCL2, and CCL3 is associated with reduced infiltration of neutrophils in tumors. Increased expression of CCL24 in CD200R-deficient tumors resulted in infiltration of eosinophils, which contributes to anti-tumor activity. In a recent publication,[20] we reported that CD200R-deficiency resulted in up-regulation of CCL8 in a different tumor model. Thus, regulation of production of chemokines in myeloid cells in TME appears to be a general function of the CD200-CD200R pathway.

In this study, we found that CD200R-deficiency resulted in the reduction of neutrophil infiltration in both tumor models. Downregulation of CXCL3, CXCL2, and CCL3 in TAMs and neutrophils (Figure 4) explains why neutrophils were dramatically reduced in TME of CD200R-deficient tumors. These chemokines, especially the first two chemokines, are known to interact with CXCR2 on neutrophils to recruit neutrophils.[21–23] In both mouse and human scRNA-seq datasets, expression of these chemokines has a positive correlation with CD200R in TAMs (Figure S4) and is associated with more CD33 (a biomarker for human neutrophils) expression in a metastatic melanoma RNA-seq dataset (Figure S5). The mechanisms for the downregulation of CXCL3, CXCL2, and CCL3 in TAMs and neutrophils are not entirely clear at this stage. It seems that inhibition of ERK activation restores the expression of these chemokine genes, suggesting that increased activation of ERK in CD200R-deficient TAMs and neutrophils is responsible for reduced expression of these chemokines. In addition to reduced recruitment, we also observed that CD200R-deficient neutrophils lost tumor promoting functions (Figure 3H). Neutrophils enhance tumor-associated inflammation/angiogenesis,[24,25] activating tumor invasion/metastasis,[26] and regulating tumor-specific T cell

responses[27,28] through a number of mechanisms, including the production of inflammatory mediators such as S100A8/9 and IL-1β (Figure S6) and other tumor promoting enzymes.[29] The reduction of neutrophils together with their functional impairment in TME of CD200R-deficient tumors, therefore, is a significant factor that contributes to the slower tumor growth.

Eosinophils accumulate in certain types of tumors as part of an immune response to cancer cells.[30] However, the exact role of eosinophils in cancer is not fully understood. Some studies have suggested that eosinophils may have anti-tumor properties through direct tumor cell killing via production of anti-tumor factors such as TNF-α[31] and other effector proteins,[32] and promoting recruitment of anti-tumor $CD8^+$ T cells into tumors through blood vessel normalization and production of chemokines such as CXCL9 and CXCL10 [19], while others have suggested that they may contribute to tumor growth and progression[33,34] through mechanisms such as promoting tumor cell proliferation[33] and production of IL-13 to promote M2 macrophage differentiation.[34] In this work, we observed significantly increased tumor infiltration of eosinophils in CD200R-deficient tumors. We found that neutralizing CCL24 reduced numbers of eosinophils in tumors, and anti-CCL24 or anti-SiglecF treatment significantly accelerated tumor growth in $CD200R^{-/-}$ mice (Figure 6). These observations suggest that TAM-derived CCL24 recruits eosinophils into tumors in $CD200R^{-/-}$ mice, which contributes to anti-tumor activity. However, we also observed that a notable difference between eosinophils in tumors and peripheral lymphoid organs is the lack of CCR3 expression in tumor eosinophils (Figure 6C). This data suggests that the function of CCL24 in TME may be limited to recruiting peripheral eosinophils into tumors but lacks direct functional impacts on tumor eosinophils. Although at this stage, we do not know the exact mechanisms of how eosinophils inhibit tumor growth in our experimental system, we believe that they may do so by 1) direct tumor cell killing by production of anti-tumor factors such as TNF and other effector molecules, and 2) enhancing the recruitment of anti-tumor T cells by normalization of tumor vasculature and producing chemokines. Recruitment of anti-tumor T cells not only results in direct tumor cell killing but also serve as a source of TNF-α and IFN-γ, which in turn will further activate eosinophils to promote their anti-tumor activity.[19,34]

In addition to reduction of neutrophils and increased infiltration of eosinophils, TME analyses using scRNA-seq and flow cytometry also revealed that tumors in $CD200R^{-/-}$ mice overall had more infiltration of immune effector cells including $CD4^+$ and $CD8^+$ T cells, and NK cells. Although no significant percentages and functional changes were observed in these cell types, depletion experiments revealed that $CD4^+$ T cells, and $CD8^+$ T cells and NK cells together are crucial in inhibiting tumor growth in $CD200R^{-/-}$ mice. Thus, the overall increased infiltration of immune effectors in CD200R-deficient tumors contributes to inhibition of tumor growth. We consider that the following mechanisms contribute to increased accumulation of T and NK cells. First, increased expression of chemokines such as CCL8 and CCL24 may contribute to increased infiltration of immune effectors in CD200R-deficient tumors directly or indirectly. CCL24 is a chemokine that is mainly chemotactic to eosinophils[18] but also to resting T cells.[35] CCL8, also known as MCP-2,[36] has much broader functions, as it can attract monocytes, T lymphocytes, natural killer cells (NK), basophils, mast cells, and eosinophils.[37] Second, increased eosinophils and reduced neutrophils numbers and functions may also contribute to more T and NK cell accumulation in CD200R-deficient tumors. As discussed above, eosinophils were shown to promote T cell accumulation in tumors,[19] while neutrophils can have an immunosuppressive role in cancer that promotes tumor growth, primarily by dampening the recruitment of other immune cells.[38] It is intriguing that we did not observe significant functional differences between WT and CD200R-deficient T and NK cells (Figure 7) despite reduced neutrophils. We do not rule out the possibility that the intrinsic effects of CD200R-deficiency in T and NK cells may impact their phenotypes. Additionally, CD200R signaling in other cell types such as Tregs may also impact the functions of effector T cells.

In this work, we used the human-relevant $CD200^+$ NB9464D and Yummer 1.7 tumor models to evaluate the role of the CD200-CD200R pathway in the TME and its relevance in tumor growth. We found that in $CD200R^{-/-}$ mice, both tumor types grew significantly slower than in wild type mice. The slower tumor growth observed in these two models is inconsistent with our previous observations in the B16 melanoma model, where B16-CD200 tumors grew faster in $CD200R^{-/-}$ mice.[39] Similarly, we recently observed that Yumm1.7 tumors also grew faster in $CD200R^{-/-}$ mice.[20] At this stage, we do not have a definitive answer to these controversies. It seems that the two tumor models tested in this work are more immunogenic compared to the B16 and Yumm1.7 models we used previously. Another potential explanation is that

CD200R signaling in different cell types plays different roles in TME. However, this hypothesis needs to be tested using conditional deletion of CD200R in different lineages of immune cells.

Taken together, we have found that in the absence of CD200R, TAMs up-regulate CCL24 and CCL8 and down-regulate CXCL3, CXCL2, and CCL3 via activation of ERK and/or p38 MAP kinases. As a result, reduced infiltration of neutrophils and increased infiltration of eosinophils and other immune effector cells, including T and NK cells were observed in CD200R-deficient tumors. Importantly, CD200R-deficient TAMCs also showed impaired tumor promoting functions. These factors together contribute to increased anti-tumor activity in the absence of CD200R. Thus, we conclude that CD200R-mediated signaling, via interaction with CD200 on tumor cells, contributes to unfavorable TME primarily through chemokine-dependent recruitment of immune suppressive neutrophils and exclusion of anti-cancer immune effectors. Currently, blockade of CD200-CD200R pathway using antagonistic antibodies to CD200 [14] or CD200R (NCT05199272) is in clinical trials of human cancers, our data thus will provide significant insights on how this approach may work in these human trials.

STAR★METHODS

Detailed methods are provided in the online version of this paper and include the following:

- KEY RESOURCES TABLE
- RESOURCE AVAILABILITY
  - Lead contact
  - Materials availability
  - Data and code availability
- EXPERIMENTAL MODEL AND SUBJECT DETAILS
  - Mice and tumor establishment
- METHOD DETAILS
  - Single cell RNA sequencing and data analysis
  - Antibodies and flow cytometry
  - ELISA
  - Real-time PCR
  - Generation of bone marrow derived macrophages and co-culture with tumor cells
  - *In vivo* tumor promotion assay
  - Treatment of mice with established tumors
- QUANTIFICATION AND STATISTICAL ANALYSIS

SUPPLEMENTAL INFORMATION

Supplemental information can be found online at https://doi.org/10.1016/j.isci.2023.106904.

ACKNOWLEDGMENTS

The authors received funding supports from the National Cancer Institute (R01CA211014 to XF.B., T32CA090223 to F.T.). This project was supported by the OSUCCC Biostatistics and Analytical Cytometry supported in part by NCI grant P30 CA016058.

AUTHOR CONTRIBUTIONS

Conceptualization: XF.B., CH.L., and F.T.; Methodology: XF.B., CH.L., F.T., and J.Z.; Investigation: CH.L., F.T., Y.L., J.Z., JQ.L., and B.Z. ; Single cell sequencing: Y.L., X.C., P.Y., and Q.M. ; Validation: XF.B., S.B., X.P., W.C., G.X., H.W., R.W.,and Z.L.; Manuscript writing: XF.B., CH.L., and F.T.

DECLARATION OF INTERESTS

The authors declare no competing interests.

Received: October 28, 2022
Revised: March 31, 2023
Accepted: May 12, 2023
Published: May 19, 2023

REFERENCES

1. Barclay, A.N., Clark, M.J., and McCaughan, G.W. (1986). Neuronal/lymphoid membrane glycoprotein MRC OX-2 is a member of the immunoglobulin superfamily with a light-chain-like structure. Biochem. Soc. Symp. *51*, 149–157.

2. Wright, G.J., Cherwinski, H., Foster-Cuevas, M., Brooke, G., Puklavec, M.J., Bigler, M., Song, Y., Jenmalm, M., Gorman, D., McClanahan, T., et al. (2003). Characterization of the CD200 receptor family in mice and humans and their interactions with CD200. J. Immunol. *171*, 3034–3046. https://doi.org/10.4049/jimmunol.171.6.3034.

3. Zhang, S., Cherwinski, H., Sedgwick, J.D., and Phillips, J.H. (2004). Molecular mechanisms of CD200 inhibition of mast cell activation. J. Immunol. *173*, 6786–6793.

4. Mihrshahi, R., Barclay, A.N., and Brown, M.H. (2009). Essential roles for Dok2 and RasGAP in CD200 receptor-mediated regulation of human myeloid cells. J. Immunol. *183*, 4879–4886. https://doi.org/10.4049/jimmunol.0901531.

5. Minas, K., and Liversidge, J. (2006). Is the CD200/CD200 receptor interaction more than just a myeloid cell inhibitory signal? Crit. Rev. Immunol. *26*, 213–230.

6. Mihrshahi, R., and Brown, M.H. (2010). Downstream of tyrosine kinase 1 and 2 play opposing roles in CD200 receptor signaling. J. Immunol. *185*, 7216–7222. https://doi.org/10.4049/jimmunol.1002858.

7. Jenmalm, M.C., Cherwinski, H., Bowman, E.P., Phillips, J.H., and Sedgwick, J.D. (2006). Regulation of myeloid cell function through the CD200 receptor. J. Immunol. *176*, 191–199.

8. Hoek, R.M., Ruuls, S.R., Murphy, C.A., Wright, G.J., Goddard, R., Zurawski, S.M., Blom, B., Homola, M.E., Streit, W.J., Brown, M.H., et al. (2000). Down-regulation of the macrophage lineage through interaction with OX2 (CD200). Science *290*, 1768–1771.

9. Snelgrove, R.J., Goulding, J., Didierlaurent, A.M., Lyonga, D., Vekaria, S., Edwards, L., Gwyer, E., Sedgwick, J.D., Barclay, A.N., and Hussell, T. (2008). A critical function for CD200 in lung immune homeostasis and the severity of influenza infection. Nat. Immunol. *9*, 1074–1083.

10. Simelyte, E., Alzabin, S., Boudakov, I., and Williams, R. (2010). CD200R1 regulates the severity of arthritis but has minimal impact on the adaptive immune response. Clin. Exp. Immunol. *162*, 163–168. https://doi.org/10.1111/j.1365-2249.2010.04227.x.

11. Liu, J.Q., Hu, A., Zhu, J., Yu, J., Talebian, F., and Bai, X.F. (2020). CD200-CD200R pathway in the regulation of tumor immune microenvironment and immunotherapy. Adv. Exp. Med. Biol. *1223*, 155–165. https://doi.org/10.1007/978-3-030-35582-1_8.

12. Xin, C., Zhu, J., Gu, S., Yin, M., Ma, J., Pan, C., Tang, J., Zhang, P., Liu, Y., Bai, X.F., et al. (2020). CD200 is overexpressed in neuroblastoma and regulates tumor immune microenvironment. Cancer Immunol. Immunother. *69*, 2333–2343. https://doi.org/10.1007/s00262-020-02589-6.

13. Petermann, K.B., Rozenberg, G.I., Zedek, D., Groben, P., McKinnon, K., Buehler, C., Kim, W.Y., Shields, J.M., Penland, S., Bear, J.E., et al. (2007). CD200 is induced by ERK and is a potential therapeutic target in melanoma. J. Clin. Invest. *117*, 3922–3929. https://doi.org/10.1172/JCI32163.

14. Mahadevan, D., Lanasa, M.C., Farber, C., Pandey, M., Whelden, M., Faas, S.J., Ulery, T., Kukreja, A., Li, L., Bedrosian, C.L., et al. (2019). Phase I study of samalizumab in chronic lymphocytic leukemia and multiple myeloma: blockade of the immune checkpoint CD200. J. Immunother. Cancer *7*, 227. https://doi.org/10.1186/s40425-019-0710-1.

15. Kroesen, M., Nierkens, S., Ansems, M., Wassink, M., Orentas, R.J., Boon, L., den Brok, M.H., Hoogerbrugge, P.M., and Adema, G.J. (2014). A transplantable TH-MYCN transgenic tumor model in C57Bl/6 mice for preclinical immunological studies in neuroblastoma. Int. J. Cancer *134*, 1335–1345. https://doi.org/10.1002/ijc.28463.

16. Meeth, K., Wang, J.X., Micevic, G., Damsky, W., and Bosenberg, M.W. (2016). The YUMM lines: a series of congenic mouse melanoma cell lines with defined genetic alterations. Pigment Cell Melanoma Res. *29*, 590–597. https://doi.org/10.1111/pcmr.12498.

17. Wang, J., Perry, C.J., Meeth, K., Thakral, D., Damsky, W., Micevic, G., Kaech, S., Blenman, K., and Bosenberg, M. (2017). UV-induced somatic mutations elicit a functional T cell response in the YUMMER1.7 mouse melanoma model. Pigment Cell Melanoma Res. *30*, 428–435. https://doi.org/10.1111/pcmr.12591.

18. White, J.R., Imburgia, C., Dul, E., Appelbaum, E., O'Donnell, K., O'Shannessy, D.J., Brawner, M., Fornwald, J., Adamou, J., Elshourbagy, N.A., et al. (1997). Cloning and functional characterization of a novel human CC chemokine that binds to the CCR3 receptor and activates human eosinophils. J. Leukoc. Biol. *62*, 667–675. https://doi.org/10.1002/jlb.62.5.667.

19. Carretero, R., Sektioglu, I.M., Garbi, N., Salgado, O.C., Beckhove, P., and Hämmerling, G.J. (2015). Eosinophils orchestrate cancer rejection by normalizing tumor vessels and enhancing infiltration of CD8(+) T cells. Nat. Immunol. *16*, 609–617. https://doi.org/10.1038/ni.3159.

20. Talebian, F., Yu, J., Lynch, K., Liu, J.Q., Carson, W.E., and Bai, X.F. (2021). CD200 blockade modulates tumor immune microenvironment but fails to show efficacy in inhibiting tumor growth in a murine model of melanoma. Front. Cell Dev. Biol. *9*, 739816. https://doi.org/10.3389/fcell.2021.739816.

21. Jablonska, J., Wu, C.F., Andzinski, L., Leschner, S., and Weiss, S. (2014). CXCR2-mediated tumor-associated neutrophil recruitment is regulated by IFN-beta. Int. J. Cancer *134*, 1346–1358. https://doi.org/10.1002/ijc.28551.

22. De Filippo, K., Dudeck, A., Hasenberg, M., Nye, E., van Rooijen, N., Hartmann, K., Gunzer, M., Roers, A., and Hogg, N. (2013). Mast cell and macrophage chemokines CXCL1/CXCL2 control the early stage of neutrophil recruitment during tissue inflammation. Blood *121*, 4930–4937. https://doi.org/10.1182/blood-2013-02-486217.

23. Rainard, P., Riollet, C., Berthon, P., Cunha, P., Fromageau, A., Rossignol, C., and Gilbert, F.B. (2008). The chemokine CXCL3 is responsible for the constitutive chemotactic activity of bovine milk for neutrophils. Mol. Immunol. *45*, 4020–4027. https://doi.org/10.1016/j.molimm.2008.06.010.

24. Jablonska, J., Leschner, S., Westphal, K., Lienenklaus, S., and Weiss, S. (2010). Neutrophils responsive to endogenous IFN-beta regulate tumor angiogenesis and growth in a mouse tumor model. J. Clin. Invest. *120*, 1151–1164. https://doi.org/10.1172/JCI37223.

25. Liang, W., and Ferrara, N. (2016). The complex role of neutrophils in tumor angiogenesis and metastasis. Cancer Immunol. Res. *4*, 83–91. https://doi.org/10.1158/2326-6066.CIR-15-0313.

26. Cools-Lartigue, J., Spicer, J., McDonald, B., Gowing, S., Chow, S., Giannias, B., Bourdeau, F., Kubes, P., and Ferri, L. (2013). Neutrophil extracellular traps sequester circulating tumor cells and promote metastasis. J. Clin. Invest. *123*, 3446–3458.

27. Germann, M., Zangger, N., Sauvain, M.O., Sempoux, C., Bowler, A.D., Wirapati, P., Kandalaft, L.E., Delorenzi, M., Tejpar, S., Coukos, G., and Radtke, F. (2020). Neutrophils suppress tumor-infiltrating T cells in colon cancer via matrix metalloproteinase-mediated activation of TGFbeta. EMBO Mol. Med. *12*, e10681. https://doi.org/10.15252/emmm.201910681.

28. Singel, K.L., Emmons, T.R., Khan, A.N.H., Mayor, P.C., Shen, S., Wong, J.T., Morrell, K., Eng, K.H., Mark, J., Bankert, R.B., et al. (2019). Mature neutrophils suppress T cell immunity in ovarian cancer microenvironment. JCI Insight *4*, e122311. https://doi.org/10.1172/jci.insight.122311.

29. Coffelt, S.B., Wellenstein, M.D., and de Visser, K.E. (2016). Neutrophils in cancer: neutral no more. Nat. Rev. Cancer *16*, 431–446. https://doi.org/10.1038/nrc.2016.52.

30. Varricchi, G., Galdiero, M.R., Loffredo, S., Lucarini, V., Marone, G., Mattei, F., Marone, G., and Schiavoni, G. (2018). Eosinophils: the unsung heroes in cancer? OncoImmunology *7*, e1393134. https://doi.org/10.1080/2162402X.2017.1393134.

31. Kataoka, S., Konishi, Y., Nishio, Y., Fujikawa-Adachi, K., and Tominaga, A. (2004). Antitumor activity of eosinophils activated by IL-5 and eotaxin against hepatocellular carcinoma. DNA Cell Biol. *23*, 549–560. https://doi.org/10.1089/dna.2004.23.549.

32. Lucarini, V., Ziccheddu, G., Macchia, I., La Sorsa, V., Peschiaroli, F., Buccione, C., Sistigu, A., Sanchez, M., Andreone, S., D'Urso, M.T., et al. (2017). IL-33 restricts tumor growth and inhibits pulmonary metastasis in melanoma-bearing mice through eosinophils. OncoImmunology *6*, e1317420. https://doi.org/10.1080/2162402X.2017.1317420.

33. Xie, F., Liu, L.B., Shang, W.Q., Chang, K.K., Meng, Y.H., Mei, J., Yu, J.J., Li, D.J., and Li, M.Q. (2015). The infiltration and functional regulation of eosinophils induced by TSLP promote the proliferation of cervical cancer cell. Cancer Lett. *364*, 106–117. https://doi.org/10.1016/j.canlet.2015.04.029.

34. Kratochvill, F., Neale, G., Haverkamp, J.M., Van de Velde, L.A., Smith, A.M., Kawauchi, D., McEvoy, J., Roussel, M.F., Dyer, M.A., Qualls, J.E., and Murray, P.J. (2015). TNF counterbalances the emergence of M2 tumor macrophages. Cell Rep. *12*, 1902–1914. https://doi.org/10.1016/j.celrep.2015.08.033.

35. Patel, V.P., Kreider, B.L., Li, Y., Li, H., Leung, K., Salcedo, T., Nardelli, B., Pippalla, V., Gentz, S., Thotakura, R., et al. (1997). Molecular and functional characterization of two novel human C-C chemokines as inhibitors of two distinct classes of myeloid progenitors. J. Exp. Med. *185*, 1163–1172. https://doi.org/10.1084/jem.185.7.1163.

36. Asano, K., Takahashi, N., Ushiki, M., Monya, M., Aihara, F., Kuboki, E., Moriyama, S., Iida, M., Kitamura, H., Qiu, C.H., et al. (2015). Intestinal CD169(+) macrophages initiate mucosal inflammation by secreting CCL8 that recruits inflammatory monocytes. Nat. Commun. *6*, 7802. https://doi.org/10.1038/ncomms8802.

37. Farmaki, E., Kaza, V., Papavassiliou, A.G., Chatzistamou, I., and Kiaris, H. (2017). Induction of the MCP chemokine cluster cascade in the periphery by cancer cell-derived Ccl3. Cancer Lett. *389*, 49–58. https://doi.org/10.1016/j.canlet.2016.12.028.

38. Giese, M.A., Hind, L.E., and Huttenlocher, A. (2019). Neutrophil plasticity in the tumor microenvironment. Blood *133*, 2159–2167. https://doi.org/10.1182/blood-2018-11-844548.

39. Liu, J.Q., Talebian, F., Wu, L., Liu, Z., Li, M.S., Wu, L., Zhu, J., Markowitz, J., Carson, W.E., 3rd, Basu, S., and Bai, X.F. (2016). A critical role for CD200R signaling in limiting the growth and metastasis of CD200+ melanoma. J. Immunol. *197*, 1489–1497. https://doi.org/10.4049/jimmunol.1600052.

40. Becht, E., McInnes, L., Healy, J., Dutertre, C.A., Kwok, I.W.H., Ng, L.G., Ginhoux, F., and Newell, E.W. (2018). Dimensionality reduction for visualizing single-cell data using UMAP. Nat. Biotechnol. *37*, 38–44. https://doi.org/10.1038/nbt.4314.

41. Waltman, L., and van Eck, N.J. (2013). A smart local moving algorithm for large-scale modularity-based community detection. Eur. Phys. J. B *86*, 471. https://doi.org/10.1140/epjb/e2013-40829-0.

42. Kuleshov, M.V., Jones, M.R., Rouillard, A.D., Fernandez, N.F., Duan, Q., Wang, Z., Koplev, S., Jenkins, S.L., Jagodnik, K.M., Lachmann, A., et al. (2016). Enrichr: a comprehensive gene set enrichment analysis web server 2016 update. Nucleic Acids Res. *44*, W90–W97. https://doi.org/10.1093/nar/gkw377.

43. Li, X., Zhang, Z., Li, L., Gong, W., Lazenby, A.J., Swanson, B.J., Herring, L.E., Asara, J.M., Singer, J.D., and Wen, H. (2017). Myeloid-derived cullin 3 promotes STAT3 phosphorylation by inhibiting OGT expression and protects against intestinal inflammation. J. Exp. Med. *214*, 1093–1109. https://doi.org/10.1084/jem.20161105.

44. Wang, L.X., Talebian, F., Liu, J.Q., Khattabi, M., Yu, L., and Bai, X.F. (2012). IL-10 contributes to the suppressive function of tumour-associated myeloid cells and enhances myeloid cell accumulation in tumours. Scand. J. Immunol. *75*, 273–281. https://doi.org/10.1111/j.1365-3083.2011.02662.x.

STAR★METHODS

KEY RESOURCES TABLE

REAGENT or RESOURCE	SOURCE	IDENTIFIER
Antibodies		
Anti-mouse CD45	BD Biosciences	Cat#565478
Anti-mouse CD3	BD Biosciences	Cat#562332
Anti-mouse CD4	Biolegend	Cat#100434
Anti-mouse CD8α	BD Biosciences	Cat#563152
Anti-mouse NK1.1	BD Biosciences	Cat#740853
Anti-mouse CD11b	eBioscience	Cat#17-0112-83
Anti-mouse CD200	Biolegend	Cat#123810
Anti-mouse CD200R	eBioscience	Cat#46-5201-82
Anti-mouse Gr-1	Biolegend	Cat#108406
Anti-mouse Ly6C	Biolegend	Cat#128006
Anti-mouse F4/80	BD Biosciences	Cat#565613
Anti-mouse Ly6G	BD Biosciences	Cat#740157
Anti-mouse SiglecF	Biolegend	Cat#155506
Anti-mouse TCRβ	Biolegend	Cat#109220
Anti-mouse CCR2	BD Biosciences	Cat#747963
Anti-mouse CD44	eBioscience	Cat#12-0441-82
Anti-mouse CD62L	eBioscience	Cat#17-0621-83
Anti-mouse Foxp3	eBioscience	Cat#12-4771-82
Anti-mouse TNF-α	BD Biosciences	Cat#563943
Anti-mouse IFN-γ	BD Biosciences	Cat#XMG1.2
Anti-mouse Granzyme B	Biolegend	Cat#396414
Anti-mouse Perforin	eBioscience	Cat#12-9392-80
Anti-mouse phospho-ERK	Biolegend	Cat#6B8B69
Anti-mouse phosepho-p38	BD Biosciences	Cat#36/p38
Anti-mouse phospho-JNK	BD Biosciences	Cat#N9-66
control IgG2a antibody	BioXcell	Cat#BE0130
Anti-mouse SiglecF depleting antibody	R&D Systems	Cat#238047
Anti-mouse CCL24 neutralizing antibody	R&D Systems	Cat#AF528
Anti-mouse CD8 depleting antibody	BioXcell	Cat#BE0004-1
Anti-mouse NK1.1 depleting antibody	BioXcell	Cat#BP0036
Anti-mouse CD4 depleting antibody	BioXcell	Cat#BE0003-1
Anti-mouse Gr1 (Biotin)	BD Biosciences	Cat#553124
Chemicals, peptides, and recombinant proteins		
SCH772984 ERK inhibitor	Cayman	Cat#19166
LY2228820 p38 inhibitor	Cayman	Cat#23259
SP600125 JNK inhibitor	Cayman	Cat#10010466
Nifuroxazide STAT inhibitor	MedChemExpress	Cat#HY-B1436
BAY11-7082 NFkB inhibitor	TCI America	Cat#T2846100MG
Critical commercial assays		
ELISA mouse CCL8 kit	Biolegend	Cat#446904
ELISA mouse CCL24 kit	Thermo Scientific	Cat#EMCCL24

(*Continued on next page*)

Continued

REAGENT or RESOURCE	SOURCE	IDENTIFIER
ELISA mouse CCL3 kit	R&D Systems	Cat#MMA00
ELISA mouse CXCL2 kit	R&D Systems	Cat#MM200
ELISA mouse CXCL3 kit	Abcam	Cat#ab272191
Biotin microbeads	Miltenyi Biotec	Cat#130090485
Deposited data		
Single cell transcriptome sequencing data	This paper	GEO:GSE211963
Experimental models: Cell lines		
NB9464D	Provided by Ruoning Wang	N/A
Yummer1.7 cells	Millipore Sigma	Cat#SCC245
Experimental models: Organisms/strains		
Mouse C57BL/6	Jackson Laboratory	2498079–86
Mouse C57BL/6 CD200R$^{-/-}$	Taconic Farms	N/A
Oligonucleotides		
Primer: CCL8, 5′-ACGCTAGCCTCCACTCCAAA-3′ (forward)	This paper	N/A
Primer: CCL8 5′-GAGCCTTATCTGGCCCAGTC-3′ (reverse)	This paper	N/A
Primer: CCL24, 5′-CATCTTGCTGCACGTCCTTT-3′ (forward)	This paper	N/A
Primer: CCL24 5′-ATGGCCCTTCTTGGTGATGA-3′ (reverse)	This paper	N/A
Primer: CCL3, 5′-GAAGATTCCACGCCAATTCATC-3′ (forward)	This paper	N/A
Primer: CCL3 5′-GATCTGCCGGTTTCTCTTAGTC-3′ (reverse)	This paper	N/A
Primer: CXCL2, 5′-TAAGCACCGAGGAGAGTAGAA-3′ (forward)	This paper	N/A
Primer: CXCL2 5′-GTCCAAGGGTTACTCACAACA-3′ (reverse)	This paper	N/A
Primer: CXCL3 CXCL3, 5′-GCACCCAGACAGAAGTCATAG-3′ (forward)	This paper	N/A
Primer: CXCL3 5′-ACTTGCCGCTCTTCAGTATC-3′ (reverse)	This paper	N/A
Software and algorithms		
Flowjo software	Tree Star	V10.8
Cell Ranger software	10x Genomics	v.6.0.1
EnrichR	Ref.[19]	v.3.1
Seurat	Satija Lab	v.4.0.5
Prism software	GraphPad	v9.5

RESOURCE AVAILABILITY

Lead contact

Further information and requests for resources and reagents should be directed to and will be fulfilled by the lead contact Xue-Feng Bai, (Xue-Feng.Bai@osumc.edu).

Materials availability

Inquiries can be directed to the lead contact, Dr. Xue-Feng Bai

Data and code availability

- Our single cell transcriptome sequencing data has been deposited in the GEO database with the accession number GSE211963.
- This paper does not report the original code.
- Any additional information required to reanalyze the data reported in this paper is available from the lead contact upon request.

EXPERIMENTAL MODEL AND SUBJECT DETAILS

Mice and tumor establishment

C57BL/6 mice were purchased from The Jackson Laboratory, and CD200R$^{-/-}$ mice were originally generated via a contract with Taconic Farms and were bred into the C57BL6 background for over 12 generations.[39] Mouse genotypes were confirmed using standard PCR genotyping or flow cytometry analysis of peripheral lymphocytes. All mice were maintained and cared for in The Ohio State University (OSU) laboratory animal facilities which are fully accredited by OSU Institutional Animal Care and Use Committee (IACUC) and in accordance with the National Institutes of Health guidelines (Guide for the Care and Use of Laboratory Animals). 8–12 weeks old adult mice were used in the present study, and male or female mice were randomized into different experimental groups before use. To establish subcutaneous (s.c.) tumors in C57BL/6 and CD200R$^{-/-}$mice, 3-4 x 10^6 NB9464D cells (provided by Ruoning Wang) or 1 × 10^6 Yummer1.7 cells (Millipore Sigma, Cat#SCC245) in 100 μl PBS were injected into each mouse s.c. The development of tumors was monitored in a blinded manner, and tumors were measured for length (a) and width (b) every two-three day using a digital caliper and tumor volumes were calculated as (a*b^2)/2.

METHOD DETAILS

Single cell RNA sequencing and data analysis

Eight weeks old WT and CD200R$^{-/-}$ male C57BL/6 mice were inoculated s.c. with 3 × 10^6 NB9464D tumor cells. On day 28 post inoculation, single cell suspensions were prepared from the tumors after mechanical disruption and enzymatic digestion with 1 mg/mL Type IV Collagenase (Sigma). Live total tumor cells or CD45$^+$ infiltrating leukocytes were sorted on a BD FACSAria Ilu Cell Sorter and immediately processed for scRNA-seq. Experimental procedures for scRNA-seq followed established techniques using the Chromium Next GEM Single Cell 3′ Kit v3.1 (10x Genomics). Briefly, total tumor cells or FACS-sorted CD45$^+$tumor infiltrating leukocytes were loaded onto a Chromium Next GEM Genomics Chip G and emulsified with Chromium Next GEM Single Cell 3′ Gel Bead (v3.1) using a Chromium Controller. Libraries were constructed from the barcoded cDNAs (Genomics Shared Resources, Ohio State University Comprehensive Cancer Center) and sequenced for approximately 300 million reads/samples on a NovaSeq SP flow cell (Illumina) at the Core facility (Ohio State University Comprehensive Cancer Center).

Using the Cell Ranger software (v.6.0.1), we converted BCL files into FASTQ files, trimmed adapters and primer sequences, mapped reads to the mm10 reference genome, and quantified expression levels. In this step, to eliminate low-quality and dying cells, we filtered out cells with counts less than 200 and those with >5% mitochondrial counts. Then, we used the Seurat software (v.4.0.5) for the downstream analysis, based on the count data obtained from Cell Ranger. Specifically, we normalized counts using the LogNormalize approach (i.e., the NormalizeData function), found variable genes via the FindVariableFeatures function, integrated multiple samples utilizing the functions of SelectIntegrationFeatures, FindIntegrationAnchors, and IntegrateData, reduced dimensionality by Principal Component Analysis (PCA), visualized cells in a low-dimensional space using the Uniform Manifold Approximation and Projection (UMAP) algorithm,[40] and determined cell clusters using the shared nearest neighbor (SNN) modularity optimization based clustering algorithm.[41] Moreover, we performed pathway enrichment analysis using enrichR[42] (v.3.1).

Antibodies and flow cytometry

Fluorescence labeled monoclonal antibodies to mouse CD45 (30-F11, 565478, BD Biosciences), CD3 (145-2c11, 562332, BD Biosciences), CD4 (GK1.5, 100434, Biolegend), CD8α (53–6.7, 563152, BD Biosciences), NK1.1 (Pk136, 740853, BD Biosciences), CD11b (M1/70, 17-0112-83, eBioscience), CD200 (OX-90, 123810, Biolegend), CD200R (OX110, 46-5201-82, eBioscience), Gr-1 (RB6-8C5, 108406, Biolegend), Ly6C (HK1.4, 128006, Biolegend), F4/80 (T45-2342, 565613, BD Biosciences), Ly6G (1A8, 740157, BD Biosciences), SiglecF (S17007L, 155506, Biolegend), TCRβ (H57-597, 109220, Biolegend), CCR2 (475301, 747963, BD Biosciences), CD44 (IM7, 12-0441-82, eBioscience), CD62L (MEL-14, 17-0621-83, eBioscience), Foxp3 (NRRF-30, 12-4771-82, eBioscience), TNF-α (XT22, 563943, BD Biosciences), IFN-γ (XMG1.2, BD Biosciences), Granzyme B (QA18A28, 396414, Biolegend), Perforin (eBioOMAK-D, 12-9392-80, eBioscience), phospho-ERK (6B8B69, Biolegend), phosepho-p38 (36/p38, BD Biosciences) and phospho-JNK (N9-66, BD Biosciences), and isotype-matched control antibodies were purchased from Biolegend or BD Biosciences. All antibodies utilized in this work were validated prior to utilization. Mononuclear cells from tumors were prepared as we previously described.[39] For cell surface staining, cells were incubated with antibodies in 0.1 M PBS (pH7.4) supplemented with 1% FCS and 0.1% sodium azide on ice for 30 minutes. Cells were then

washed three times and fixed in 1% paraformaldehyde, followed by flow cytometry analysis. For staining of phospho-proteins (ERK, p38, and JNK), the cells were fixed and permeabilized with the permeabilization buffer (Invitrogen) for 30 min at 4°C. Subsequently, the cells were incubated with the cell surface antibodies and phospho-protein antibodies for 30 min at 4°C. For intracellular staining of TNF-α, IFN-γ, Granzyme B, Perforin, or Foxp3, cells were first stimulated with a cell stimulation cocktail (Invitrogen) for 4 hrs (TNF-α, IFN-γ) in the presence of Gorgistop (BD Biosciences) or unstimulated (Granzyme B, Perforin, Foxp3). The cells were first stained for the cell surface markers (CD4/CD8/NK1.1/TCR-b), followed by a standard intracellular cytokine staining procedure. A Celesta flow cytometer (BD) was used to detect stained cells. Data was analyzed using the flowjo software (Tree Star, Inc., OR).

ELISA

The following ELISA kits, including mouse CCL8 (MCP-2; Biolegend, Cat#446904), mouse CCL24 (Eotaxin-2; Thermo Scientific, Cat#EMCCL24), mouse CCL3 (MIP-1a; R&D Systems, Cat#MMA00), mouse CXCL2 (MIP-2; R&D Systems, Cat#MM200), and mouse CXCL3 (Abcam, Cat#ab272191), were used to quantify chemokines in tumor lysates or culture supernatants from BMDM/NB9464D co-cultures according to manufacturer's instructions.

Real-time PCR

Quantitative real-time PCR was done using previously determined conditions (33). The following primers were used for amplifying the chemokine genes: CCL8, 5′-ACGCTAGCCTCCACTCCAAA-3′ (forward) and 5′-GAGCCTTATCTGGCCCAGTC-3′ (reverse); CCL24, 5′-CATCTTGCTGCACGTCCTTT-3′ (forward) and 5′-ATGGCCCTTCTTGGTGATGA-3′ (reverse); CCL3, 5′-GAAGATTCCACGCCAATTCATC-3′ (forward) and 5′-GATCTGCCGGTTTCTCTTAGTC-3′ (reverse); CXCL2, 5′-TAAGCACCGAGGAGAGTAGAA-3′ (forward) and 5′-GTCCAAGGGTTACTCACAACA-3′ (reverse); CXCL3, 5′-GCACCCAGACAGAAGTCATAG-3′ (forward) and 5′-ACTTGCCGCTCTTCAGTATC-3′ (reverse). Each sample was assayed in triplicate, the relative gene expression was calculated by plotting the Ct (cycle number), and the average relative expression for each group was determined using the comparative method ($2^{-\Delta\Delta Ct}$).

Generation of bone marrow derived macrophages and co-culture with tumor cells

Bone marrow (BM) cells from C57BL/6 and CD200R$^{-/-}$ mice were plated in 15 cm culture dishes in DMEM medium containing 10% FBS and M-CSF (50 ng/ml) or L929-conditioned medium as described.[43] The cells were allowed to grow in an incubator at 37°C for 3 days. On day 3, fresh culture medium was added to the plate and allowed to grow for another 2 days. Macrophages (adherent cells) were dissociated on day 5 using 5 mM EDTA and re-suspended in DMEM medium containing 10% FBS. The macrophages ($1x10^6$ cells/ml) were then co-cultured with NB9464D tumor cells at 1:1 ratio. 24 and 48 hours later, culture supernatants were collected for ELISA. The detached cells were used for flow cytometry analysis or qPCR for chemokine gene expression analysis. For some experiments, inhibitors of ERK (SCH772984, 1 μM), p38 (LY2228820, 5 μM), and JNK (SP600125, 5 μM) were added to the co-cultures.

In vivo tumor promotion assay

Ly6G$^+$ neutrophils were used to mix with were purified from bone marrow cells from WT and CD200R$^{-/-}$ mice using Biotin-anti-Gr1 (RB6-8C5; BD Biosciences) followed by magnetic antibody cell separation using anti-biotin microbeads (Miltenyi Biotec, Auburn, CA) as we previously described.[44] NB9464D cells were mixed with BMDMs or Ly6G$^+$ neutrophils at a 1:1 ratio and 6 million mixed cells or 3 million NB9464D cells were injected into each recipient mouse s.c. Tumor growth was monitored by measuring tumor length and width every 2 days after the appearance of tumors.

Treatment of mice with established tumors

We first established NB9464D tumors in male or female CD200R$^{-/-}$ mice by injecting 3×10^6 NB9464D cells in 100 μl PBS. When tumors are palpable (typically 14 days after tumor cell injection), mice were treated with 15 μg/mouse of anti-SiglecF (238047, R&D Systems) or a control IgG2a antibody (BioXcell) every other day. This dose of anti-SiglecF has been shown to be sufficient to deplete Eosinophils.[19] Similarly, some CD200R$^{-/-}$ mice with established NB9464D tumors were treated with 25 μg/mouse of anti-CCL24 neutralizing antibody (R&D Systems, Cat#AF528) or a control antibody (Cat#BE0130, BioXcell) every other day. In some experiments, mice were treated with anti-CD4 (GK1.5, BE0003-1, BioXcell), anti-CD8 (53-6.7,

BE0004-1, BioXcell), anti-NK1.1 (PK136, BP0036, BioXcell) or anti-CD8+anti-NK1.1 twice weekly to deplete CD4, CD8 and/or NK cells in tumor bearing mice.

QUANTIFICATION AND STATISTICAL ANALYSIS

Statistical analyses were performed using GraphPad Prism 9.5 software (GraphPad Software Inc, La Jolla, CA, USA). All continuous data were presented as mean $\pm$ standard error of the mean (SEM) unless otherwise indicated. The differences between the treatments and the untreated control were compared using two sample t-tests (assuming unequal variance) for continuous data with proper data transformation as needed or one way ANOVA. $p < 0.05$ was considered statistically significant. Sample size of 5–6 mice per group was used and replicate experiments were conducted to ensure the technical reproducibility. Sample size of 5 per group provided at least 80% power to detect an effect size of 2 between the two groups assuming the coefficient of variance $\leq$35% at significance level of 0.05. Two proportion *z*-test was used for the scRNAseq data to compare number differences between cell clusters in tumors from WT versus CD200R$^{-/-}$ mice. Wilcoxon rank sum test was used to compare expression of chemokine genes (scRNA-seq) between tumors from WT and CD200R$^{-/-}$ mice.